BJ www.biochemj.org

BJ Cell

Biochem. J. (2009) **417**, 195–203 (Printed in Great Britain) doi:10.1042/BJ20081073

Atp6v1c1 is an essential component of the osteoclast proton pump and in F-actin ring formation in osteoclasts

Shengmei FENG*†, Lianfu DENG‡, Wei CHEN†§, Jianzhong SHAO*, Guoliang XU‖ and Yi-Ping LI*†‡§¶[1]

*Life Science College, Zhejiang University, 388 Yuhang Road, Hongzhou 310058, People's Republic of China, †Department of Cytokine Biology, The Forsyth Institute, 140 The Fenway, Boston, MA 02115, U.S.A., ‡Shanghai Institute of Traumatology and Orthopaedics, 197 Rui Jin Er Road, Shanghai 200025, People's Republic of China, §Department of Developmental Biology, Harvard School of Dental Medicine, 188 Longwood Avenue, Boston, MA 02115, U.S.A., ‖Institute of Biochemistry and Cell Biology, Shanghai Institute for Biological Sciences, Chinese Academy of Sciences, 320 Yueyang Road, Shanghai 200031, People's Republic of China, and ¶Zhejiang Cell Biomedical Research College, 48 Changsheng Road, Hangzhou 310006, People's Republic of China

Bone resorption relies on the extracellular acidification function of V-ATPase (vacuolar-type proton-translocating ATPase) proton pump(s) present in the plasma membrane of osteoclasts. The exact configuration of the osteoclast-specific ruffled border V-ATPases remains largely unknown. In the present study, we found that the V-ATPase subunit Atp6v1c1 (C1) is highly expressed in osteoclasts, whereas subunits Atp6v1c2a (C2a) and Atp6v1c2b (C2b) are not. The expression level of C1 is highly induced by RANKL [receptor activator for NF-κB (nuclear factor κB) ligand] during osteoclast differentiation; C1 interacts with Atp6v0a3 (a3) and is mainly localized on the ruffled border of activated osteoclasts. The results of the present study show for the first time that C1-silencing by lentivirus-mediated RNA interference severely impaired osteoclast acidification activity and bone resorption, whereas cell differentiation did not appear to be affected, which is similar to a3 silencing. The F-actin (filamentous actin) ring formation was severely defected in C1-depleted osteoclasts but not in a3-depleted and a3$^{-/-}$ osteoclasts. C1 co-localized with microtubules in the plasma membrane and its vicinity in mature osteoclasts. In addition, C1 co-localized with F-actin in the cytoplasm; however, the co-localization chiefly shifted to the cell periphery of mature osteoclasts. The present study demonstrates that Atp6v1c1 is an essential component of the osteoclast proton pump at the osteoclast ruffled border and that it may regulate F-actin ring formation in osteoclast activation.

Key words: acidification, Atp6v1c1 (C1), bone resorption, filamentous actin (F-actin) ring, osteoclast, vacuolar-type proton-translocating ATPase (V-ATPase).

INTRODUCTION

V-ATPases (vacuolar-type proton-translocating ATPases) are composed of an ATP-hydrolytic domain (V_1) and a proton-translocation domain (V_0), as well as the accessory subunits ac45 and M8-9 [1]. The V_1 domain is located in the cytoplasm and contains eight different subunits (A–H): the catalytic nucleotide-binding subunit A, the non-catalytic nucleotide-binding subunit B (stoichiometry of A3:B3), and the stalk subunits C–H (proposed stoichiometry of C1:D1:E1:F1:G2:H1) [2–4]. The V_0 domain, an integral membrane-bound domain, connects to the V_1 domain by the central and peripheral stalks. In mammals, the V_0 domain consists of a, c, c′, c″, e and d subunits. V-ATPases are involved in a wide variety of physiological processes, including endocytosis, intracellular membrane trafficking, macromolecular processing and degradation, and ligand-coupled transport, but they are primarily responsible for the acidification of intracellular compartments in all eukaryotic cells [3,5]. For their diverse functions, V-ATPases utilize specific subunit isoform(s) in specific cells and cell organelles. For instance, a4, B1, C2b, d2 and G3 are highly expressed in the kidney and epididymis [6–10]; a1 and G2 are highly expressed in the brain [11]; and a3, B2 and d2 are highly expressed in osteoclasts [9,12,13]. Osteoclasts are the principal cells responsible for bone resorption. Their ruffled membrane V-ATPases tightly coupled to a passive chloride channel are required for acidification of the resorption lacunae and bone matrix demineralization [14]. Therefore we reason that osteoclast V-ATPases present in the ruffled border are comprised of unique subunits such as a3, B2 and other unknown subunits, which are different from other V-ATPases [12,15]. In the present study, we defined another subunit of the osteoclast proton pump.

It is known that in mouse V-ATPase there are three isoforms of subunit C: Atp6v1c1 (C1), Atp6v1c2a (C2a) and Atp6v1c2b (C2b). C1 is expressed ubiquitously, but C2a is a lung-specific isoform containing a 46-amino-acid insertion and C2b is a kidney-specific isoform without the insert [10,16]. Despite these insights, the possible role of C1 as an essential component of the osteoclast proton pump, the function of C1 in an osteoclast proton pump, its localization in activated osteoclasts, and its function in the differentiation, maturation, acidification and bone resorption of mature osteoclasts, remain unclear.

In multinucleated osteoclasts, bone resorption is active in the ruffled border surrounded by a tight sealing zone, which contains highly dynamic actin-containing adhesion structures known as podosomes. These podosomes are composed of a small F-actin (filamentous actin) column surrounded by proteins such as vinculin and paxillin. Protons and enzyme secretions are restricted to the resorption lacuna, limited by the sealing zone; however, in mature osteoclasts seeded on to glass or plastic, podosomes form a belt on the cell periphery [17–19]. Previous reports showed

Abbreviations used: BMM, bone marrow-derived monocyte; co-IP, co-immunoprecipitation; DAPI, 4′,6-diamidino-2-phenylindole; ES cell, embryonic stem cell; F-actin, filamentous actin; FBS, fetal bovine serum; GFP, green fluorescent protein; HEK, human embryonic kidney; HRP, horseradish peroxidase; M-CSF, macrophage colony-stimulating factor; α-MEM, α-modified Eagle's medium; MNC, multinucleated cell; OCL, osteoclast-like cell; RANKL, receptor activator for NF-κB (nuclear factor κB) ligand; RNAi, RNA interference; RT, reverse transcription; shRNA, short hairpin RNA; siRNA, small interfering RNA; TR, Texas Red; TRAP, tartrate-resistant acid phosphatase; V-ATPase, vacuolar-type proton-translocating ATPase.

[1] To whom correspondence should be addressed (email ypli@forsyth.org).

that the formation of actin sealing rings was severely impaired in osteoclasts deficient in Atp6v0d2 [20], whereas formation was uncertain in Atp6v0a3-deficient osteoclasts [21,22]. These results prompted us to wonder whether V-ATPase subunits are also involved in F-actin ring formation during osteoclast activation. Previously, Vitavska et al. [23,24] reported that *in vitro* subunit C can directly bind and stabilize F-actin, increase the initial rate of actin polymerization in a concentration-dependent manner and cross-link actin filaments to bundles of varying thickness. According to these findings we speculate that subunit C1 may be involved in F-actin ring formation during osteoclast activation.

In the present study we show that subunit C1 is highly expressed in mouse osteoclasts and that its expression can be induced by RANKL [receptor activator of NF-κB (nuclear factor κB) ligand] and M-CSF (macrophage colony-stimulating factor) during osteoclast differentiation. The acidification activity and the bone resorption function of C1-depleted cells were severely impaired, but osteoclast differentiation and maturation were normal. Furthermore, immunohistochemistry showed that C1 was expressed mainly in the ruffled membrane. The co-IP (co-immunoprecipitation) assay showed that C1 interacts with subunit a3 and that C1 co-localized with microtubules in the plasma membrane and its vicinity in mature osteoclasts. We also found that F-actin ring formation was severely defected in C1-depleted osteoclasts and that C1 co-localized with F-actin both in the cell periphery and in the cytoplasm of mature osteoclasts.

EXPERIMENTAL

Animal experimentation

All animal experimentation was carried out according to the legal requirements of the Association for Assessment and Accreditation of the Laboratory Animal Care International and the Institution Care and Use Commitee of The Forsyth Institute (Boston, MA, U.S.A.).

Cells and cell culture

The mature osteoclasts in primary culture were generated from BMMs (bone marrow-derived monocytes) as described [25]. Briefly, BMMs were isolated from tibiae and femurs from six-week-old C57BL6 mice. BMMs ($1–2 \times 10^5$) were seeded into a well of a 24-well plate and 1×10^6 BMMs were seeded into a well of a six-well plate. The cells were cultured in α-MEM (α-modified Eagle's medium) containing 10 % (v/v) FBS (fetal bovine serum), 10 ng/ml RANKL and 10 ng/ml M-CSF at 37 °C in a humidified atmosphere containing 5 % CO_2 for 4–6 days. As a control, a monocytic osteoclast progenitor cell line, MOCP-5, that was generated in our laboratory [26], was also induced into multinuclear OCLs (osteoclast-like cells) in α-MEM containing 10 % (v/v) FBS, 10 ng/ml RANKL and 10 ng/ml M-CSF for 4 days [26].

GeneChip analysis

Total RNA was extracted from human osteoclastoma and stromal cells using TRIzol® reagent (Life Technologies), according to the manufacturer's protocol. GeneChip analysis was performed by the Microarray Core Facility at Harvard Medical School (Boston, MA, U.S.A.). In brief, equivalent amounts of mRNA from osteoclastoma and stromal cells were reverse-transcribed into cDNA, labelled with reporter molecules [Cy3 (indocarbocyanine) and Cy5 (indodicarbocyanine)], and tested by simultaneously hybridizing the two cDNAs probes to a DNA microarray. The data were analysed using an Affymetrix GeneChip scanner and accompanying gene expression software. We compared the signal intensity of Atp6v1c1 and Atp6v1c2 in human osteoclast samples. A comparison of Atp6v1c1 in stromal cells and human osteoclast samples was derived from the resulting intensity ratios.

Preparation of RNA samples and RT (reverse transcription)–PCR analysis

Total RNA was isolated from cultured cells or mouse tissues with TRIzol® reagent (Invitrogen) according to the manufacturer's protocol. Mouse cDNA was reverse-transcribed from 0.5 μg of total RNA with oligo$(dT)_{15}$ primer by AMV (avian myeloblastosis virus) reverse transcriptase (Promega) following the manufacturer's standard method. Then, 10 % of the resulting cDNA was used for cloning the 1.15 kb full-length coding sequence of *Atp6v1c1* (GenBank® accession no. NM_025494.2) with the following primers: *c1-cds-F* 5′-CGCGGATCCAACATGACTGAGTTCTGGCTC-3′ and *c1-cds-R* 5′-CCGCTCGAGTTACTTGAATTCCAGCAAGTTG-3′. Each RT–PCR assay was performed with an aliquot of 2 % of the resulting cDNA with gene-specific primers as follows: for *Atp6v1c1* (expected product of 523 bp) sense 5′-AATAATCTTGCCGTCTCTTCC-3′ and antisense 5′-GCGTTTCATACTGCTTAATCC-3′; for *Atp6v1c2* (common primers for c2-a and c2-b; expected product of 433 bp) sense 5′-AACTTCAAAGTCTAACCTGTCC-3′ and antisense 5′-GACAATATCGCTCAGTGTCC-3′; and for *β-actin* (expected product of 517 bp) sense 5′-CATTGAACATGGCATTGTTACC-3′ and antisense 5′-CAGCTCATAGCTCTTCTCCAGG-3′. All RT–PCR assays were repeated three times. The product fragments were resolved by electrophoresis in a 1 % agarose gel. Semi-quantitative analysis was performed with Labworks 4.6 software.

Preparation of antibodies

Rabbit antibodies against synthetic peptides: Atp6v1c1 E^{12}KTCQQTWEKLHAATTK^{28} [16], a3 F^{816}YSGTGYKLSPFTFTVDSD^{834} and Atp6v1a Q^{603}LLEDMQNAFRSLED^{617} [8] were generated by coupling peptides to KLH (haemocyanin from Keyhole Limpet) and immunizing rabbits. The monoclonal antibodies against GAPDH (14C10; glyceraldehyde-3-phosphate dehydrogenase), anti-rabbit IgG and anti-mouse IgG [HRP (horseradish peroxidase)-linked] were purchased from Cell Signaling. Anti-FLAG M2, anti-GFP (green fluorescent protein) and anti-actin monoclonal antibodies were purchased from Sigma. Goat-anti-rabbit-FITC and goat-anti-mouse-TR (where TR is Texas Red) were purchased from Santa Cruz Biotechnology.

Selection of siRNA (small interfering RNA) and Western blot analysis

siRNA was designed from the Dharmacon siDESIGN centre (http://www.dharmacon.com) specifically targeting mRNA of *Atp6v1c1* with the sequences of c1s1 5′-TTCGTGACTTCCAGTATAA-3′, c1s2 5′-TTGCGTGGATTCATATAAA-3′ and c1s3 5′-GAGTTGACTTGGTTACTTA-3′, and specifically targeting mRNA of *Atp6v0a3* with the sequence of si-a3 5′-GTATCCTCATTCACTTCAT-3′. The negative control siRNA targeting LacZ (termed si-LacZ) is 5′-CTCGGCGTTTCATCTGTGG-3′. The shRNA (short hairpin RNA) oligos were annealed and ligated into the BglII/HindIII-site of pSUPER. The shRNA was then validated by determining the depletion effect on the expression of co-transfected FLAG-C1 in HEK (human embryonic kidney)-293T cells. Briefly, the resulting plasmid constructs were co-transfected into HEK-293T cells with the plasmid of FLAG-C1 using Lipofectamine™ reagent (Invitrogen) in duplicate on three independent occasions. Cells were harvested into standard lysis buffer [50 mM Tris/HCl (pH 6.8), 100 mM DTT (dithiothreitol),

2 % (w/v) SDS, 0.001 % Bromophenol Blue and 10 % (w/v) glycerol]. SDS/PAGE and Western blot analysis were carried out according to a standard protocol with the anti-FLAG monoclonal antibody (1:10000), anti-β-actin monoclonal antibody (1:3000) and anti-GFP monoclonal antibody (1:10000).

Preparation of lentivirus and infection

The effective H1 promoter shRNA expression cassettes, c1s3, si-a3 and si-LacZ, were subcloned into the lentivirus transfer vector pLB (Addgene) [27]. This was co-transfected with the packaging plasmids, pCMV-Dr8.2 and pCMV-VSV-G (Addgene) [28], into HEK-293T cells using a calcium phosphate co-precipitation method. The medium was replaced with fresh DMEM (Dulbecco's modified Eagle's medium) after co-transfection for 8 h. The lentiviral supernatant was harvested after 48–72 h and titres were determined by infecting HEK-293T cells with serial dilutions of concentrated lentivirus in the presence of 4 μg/ml polybrene (Sigma). For depletion of C1 in osteoclasts, BMMs were induced with M-CSF/RANKL for 48 h and then transduced with lentiviral supernatant for 8 h. The medium was replaced with fresh α-MEM containing 10 % (v/v) FBS, 10 ng/ml RANKL and 10 ng/ml M-CSF for primary culture. Osteoclasts were harvested for Western blot analysis or for functional experiments 3.5 days after infection.

TRAP (tartrate-resistant acid phosphatase) staining

TRAP staining was used as a marker for mature osteoclasts. Cells were fixed and stained for TRAP activity using a leukocyte acid phosphatase kit (Sigma). Pre-osteoclasts and mature multinucleated osteoclasts (more than three nuclei) appeared dark red and were counted by light microscopy. The experiment was performed in duplicate on five independent occasions. Ten fields were counted for each group. All data are expressed as means $\pm$ S.D. ($n = 10$).

Pit formation assay

Bone resorption activity was assessed using a pit formation assay performed according to the method of Chen and Li [26] with slight modifications. BMMs were cultured on dentin slices in 96-well plates and infected with lentiviral siRNA after a 48 h induction by RANKL and M-CSF. After 6 days, the slices were placed for 10 min in 1 M ammonium hydroxide and were sonicated to remove the cells. The cell-free slices were stained in 1 % Toluidine Blue in 1 % sodium borate for 1 min [29]. The experiment was repeated three times. The resorption pits appeared dark blue and were viewed by light microscopy. The percentage of pit area to a 'random field of view' was counted. Three fields were counted for each group. All data are expressed as means $\pm$ S.E.M. ($n = 3$).

Acridine Orange staining

Acid production was determined using Acridine Orange as described previously [13]. Osteoclasts were incubated in α-MEM containing 5 μg/ml Acridine Orange (Sigma) for 15 min at 37 °C, washed and chased for 10 min in fresh medium without Acridine Orange. The cells were observed under a fluorescence microscope with a 490 nm excitation filter and a 525 nm arrest filter. The experiment was performed in duplicate on four independent occasions in a 24-well plate.

Cell staining for F-actin rings

Cells were fixed with 3.7 % (w/v) formaldehyde and permeabilized with 0.2 % Triton X-100. The cells were then blocked with 1 % goat serum and 3 % BSA and incubated with 2 units/ml rhodamine phalloidin (Molecular Probes) at room temperature (25 °C) for 20 min. Nuclei were visualized with 1 μg/ml DAPI (4′,6-diamidino-2-phenylindole; Sigma). The experiment was performed in duplicate on four independent occasions in a 24-well plate.

Cell immunofluorescence

BMMs were grown on 6 cm dishes and induced by RANKL and M-CSF for 5 days. Then they were fixed with 2 % (w/v) formaldehyde in PBS for 20 min, washed with PBS three times, incubated in 0.2 % Triton X-100 for 15 min, and blocked for 1 h with 10 % normal goat serum in PBS. Additionally, cells were incubated in the primary antibody (anti-Atp6v1c1, 1:50; anti-microtubules, 1:2), diluted in 1 % normal serum in PBS overnight at 4 °C, washed three times with PBS for 5 min, and incubated with either secondary antibody goat-anti-rabbit-FITC (1:50) and rhodamine phalloidin (1:100), or with goat-anti-mouse-TR (1:50) for 1 h. Cells were then washed with PBS and mounted with anti-fade mounting medium (a gift from Dr Shi-liang Ma, Department of Biomineralization, The Forsyth Institute, Boston, MA, U.S.A.). Observations were performed by epifluorescence in a Zeiss axioplan microscope. The experiments were set in triplicate on three independent occasions.

Immunohistochemistry

Immunohistochemistry was performed as described previously [13]. Briefly, mice (C57Bl/6J male; aged 6 weeks) were anaesthetized and then perfused with 4 % (w/v) paraformaldehyde in PBS (pH 7.4). Their tibiae and femora were dissected out and immersed in the same solution overnight at 4 °C. These were then sectioned at a 6 μm thickness and mounted on gelatin-coated slides. Endogenous peroxidase activity was quenched with 0.3 % hydrogen peroxide in PBS for 20 min. Non-specific background staining was blocked by incubating sections in 10 % goat serum in PBS for 20 min. Primary antibody (anti-Atp6v1c1, 1:600) was applied overnight at 4 °C The HRP avidin–biotin complex system (Rabbit Elite ABC Kit; Vector Laboratories) was used to visualize bound antibody, and sections were counterstained with 0.1 % Fast Green (VWR). The experiments were set in triplicate on three independent occasions.

Co-immunoprecipitation

BMMs were stimulated with RANKL and M-CSF for 5 days and then washed with cold PBS and lysed in a buffer containing 20 mM Tris/HCl (pH 7.4), 150 mM NaCl, 1 % Nonidet P40 and protease inhibitors (Sigma) [30]. Following centrifugation at low speed (20 min at 14000 ***g*** at 4 °C) to remove insoluble material, cell lysates were incubated at 4 °C for 2 h with anti-Atp6v1c1 (1:1000) and then incubated with protein A/G–Sepharose beads (Santa Cruz Biotechnology) overnight. The precipitates were separated by SDS/PAGE (8 % gels), followed by immunoblotting as described previously [30]. The experiment was repeated five times.

RESULTS

Atp6v1c1 is highly expressed in mouse osteoclasts

We have characterized Atp6v0a3 as an osteoclast-specific isoform of subunit a that is essential in osteoclast-mediated extracellular acidification in bone resorption [13], suggesting that additional specific subunit isoforms may exist as components of the osteoclast ruffled border V-ATPase proton pump. In the present study, we determined whether there are other specific subunit

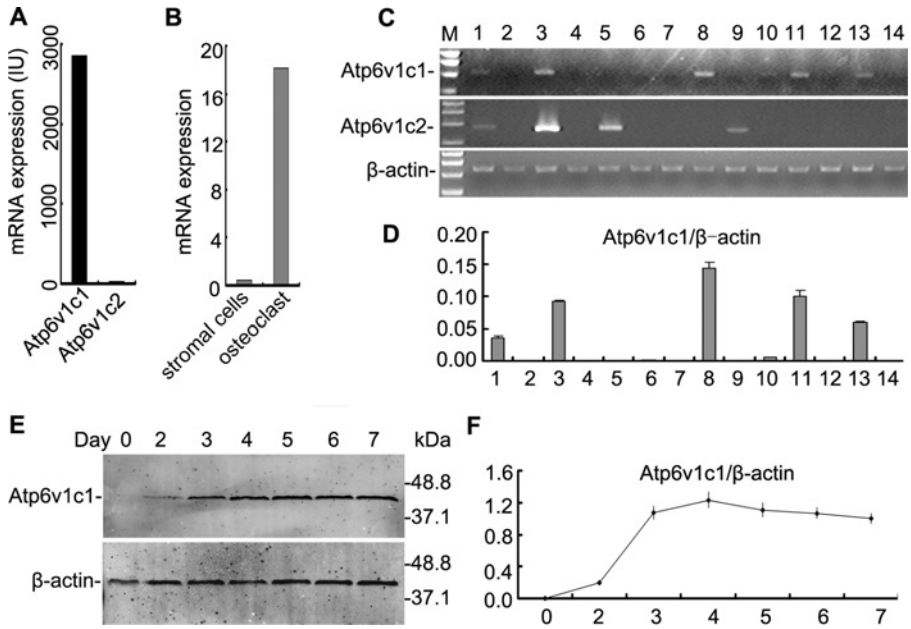

Figure 1 Expression of *Atp6v1c1* in osteoclasts

(**A**) Microarray data of expression levels of Atp6v1c1 and Atp6v1c2 in human osteoclasts. IU, international units. (**B**) Microarray data of the expression level of Atp6v1c1 in stromal cells and human osteoclasts. (**C**) Semi-quantitative RT–PCR assays in eight mouse tissues (M: molecular marker; lanes 1–8 are brain, heart, kidney, liver, lung, ovary, spleen and testis respectively) and six related cells (lanes 9–14 are ES, MOCP-5, OCLs, BMMs, osteoclast and osteoblast cells) were performed with gene-specific primers for *Atp6v1c1*, *Atp6v1c2* (the common primers for c2a and c2b) and *β-actin*. (**D**) Quantification of the *Atp6v1c1* expression level (normalized to the *β-actin* level; $n = 3$). (**E**) Time course of Atp6v1c1 protein in RANKL- (10 ng/ml) and M-CSF- (10 ng/ml) stimulated BMMs by Western blot analysis. The molecular mass (in kDa) is indicated on the right-hand side. (**F**) Quantification of Atp6v1c1 protein expression levels during osteoclast differentiation and maturation (normalized to the *β*-actin level; $n = 3$).

isoforms in the osteoclast ruffled border proton pump using microarray to analyse osteoclast mRNA gene expression profiles as described [25,31]. We found that the level of *Atp6v1c1* (*C1*) expression was approx. 139-fold higher than *Atp6v1c2* (*C2*) expression in human osteoclasts (Figure 1A), and *C1* expression in human osteoclasts was approx. 42-fold higher than that in stromal cells (Figure 1B).

Microarray data showed that *C2* was weakly expressed in osteoclasts (Figure 1A). To define whether the two isoforms of *C2* are expressed in osteoclasts, we designed primers shared by both *C2a* and *C2b* to perform semi-quantitative RT–PCR assays on eight mouse tissues and six related cell lines (Figure 1C). *C2* was detected in brain, lung, kidney and ES (embryonic stem) cells, but not in BMMs, MOCP-5 (an osteoclast precursor cell line) [26], osteoclasts or OCLs (derived from MOCP-5) (Figure 1C, middle panel). Microarray data showed that *C1* was highly expressed in osteoclasts (Figures 1A and 1B), rather than in stromal cells (Figure 1B). To verify the high expression of *C1* in osteoclasts, we performed gene-specific semi-quantitative RT–PCR. *C1* expression was not detected in osteoblasts, BMMs or MOCP-5, but it showed an induced expression in osteoclasts and OCLs. *C1* was expressed in osteoclasts at a level as strong as that of brain, kidney and testis (Figure 1C, top panel). We further quantified the expression of *C1* normalized to *β-actin*, and found that *C1* expression was highly induced by RANKL and M-CSF (approx. 16-fold; Figure 1D). To test whether C1 protein expression can also be induced by RANKL and M-CSF, BMMs were treated with RANKL and M-CSF for the time periods indicated (Figure 1E). We used Western blot analysis to detect C1 expression (Figure 1E). C1 protein was detected on day 2, continued to increase through day 4, and stayed at high levels until 7 days after stimulation with RANKL and M-CSF (normalized to the *β*-actin level; Figure 1F). These results indicated that C1 is much more highly expressed in osteoclasts than C2, and that C1 expression can be induced by RANKL and M-CSF during osteoclast differentiation.

Effective depletion of *Atp6v1c1* expression by lentiviral siRNA in osteoclasts in primary culture

Atp6v1c1 is much more highly expressed in mature osteoclasts, so we hypothesized that C1 plays an important role in osteoclast differentiation and function. To address this point, we used lentiviral constructs encoding siRNAs that target *Atp6v1c1* to infect osteoclasts in primary culture and deplete C1 expression. We first validated the effect of siRNA on cDNA of FLAG–C1 in HEK-293T cells. One of the three siRNAs (c1s3) was shown to deplete 98.8 % of the expression of FLAG–C1 in HEK-293T cells by Western blot analysis with an anti-FLAG antibody (Figures 2A and 2B), in contrast with siRNA-specific targeting to LacZ and vector. However, the other two siRNAs (c1s1 and c1s2) knocked down only approx. 27 % and 34 % of C1 expression respectively, compared with LacZ-siRNA (Figure 2B). We therefore used siRNA-c1s3 to clone into the lentivirus transfer vector pLB and to package lentivirus in HEK-293T cells for infection in the primary cultured osteoclasts after a 48 h induction by RANKL and M-CSF. Western blot analysis confirmed that the depletion of C1 was effective (Figures 2C and 2D). Lentiviral infection itself did not cause any change in C1 expression since control osteoclasts infected with LacZ-siRNA lentivirus (Lenti-LacZ; Figure 2C) showed similar protein levels as untreated osteoclasts (Mock; Figure 2C). In a3-siRNA lentivirus (Lenti-a3)-treated osteoclasts, a3 expression was knocked down by 86 %, but C1 was not knocked down and there was no difference in expression of *Atp6v1a* among the Mock, Lenti-LacZ-, Lenti-c1s3- and Lenti-a3-treated osteoclasts (Figure 2C). Taken together, these results

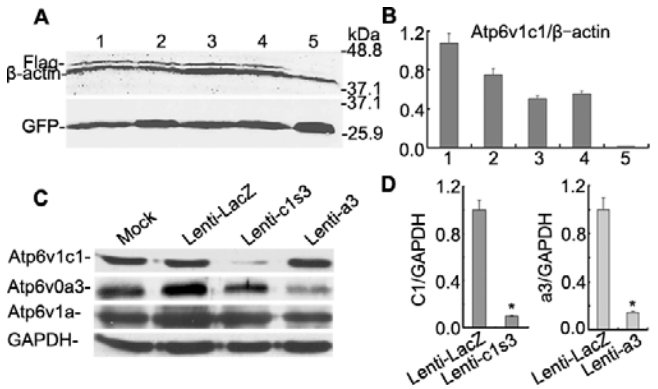

Figure 2 Validation of the depletion effect of siRNA targeting *Atp6v1c1*

(**A**) Effective siRNA target sequence selection on over-expressed FLAG-C1 in HEK-293T cells by Western blot analysis. We used anti-β-actin as a protein loading control and anti-GFP as a transfection efficiency control. Lane 1, pSUPER + FLAG-C1; Lane 2, pSUPER-LacZ + FLAG-C1; Lane 3, pSUPER-c1s1 + FLAG-C1; Lane 4, pSUPER-c1s2 + FLAG-C1; Lane 5, pSUPER-c1s3 + FLAG-C1. The molecular mass (in kDa) is indicated on the right-hand side. (**B**) Quantification of the expression of FLAG–C1 (normalized to the β-actin level) in lanes as described above ($n = 3$). (**C**) Verified c1s3 knockdown effect by lentivirus-mediated transduction of primary culture osteoclasts on day 2, induced by RANKL and M-CSF. (**D**) Quantification of the expression of Atp6v1c1 and Atp6v0a3 (normalized to the β-actin level; $n = 3$). $^*P < 0.05$ compared with that of Lenti-LacZ-treated cells.

indicate an effective and specific depletion of C1 by siRNA in primary cultured osteoclasts.

Osteoclasts depleted of Atp6v1c1 show normal cell differentiation and maturation

Lee et al. [20] reported that d2 deficiency did not affect osteoclast differentiation, but did affect pre-osteoclast fusion. Based on this finding, we wondered whether C1 could also be involved in osteoclast differentiation and maturation. To address this question, we performed a TRAP staining assay. First, for lentivirus-mediated *Atp6v1c1* knockdown, optimal viral particle numbers for infection were based on infection efficiency, determined from the percentage of target cells with GFP, which is expressed independently from the RNAi (RNA interference) sequence. We used 200 μl of lentivirus supernatant to infect 1×10^5 BMMs after a 48 h induction by RANKL and M-CSF. After another 48 h period, infected GFP$^+$ cells were viewed under fluorescence microscopy (Figure 3A). We then assessed the differentiation and maturation of *C1*-depleted osteoclasts using a TRAP staining assay 3.5 days after infection (Figure 3B). The number of stained multinuclear TRAP$^+$ osteoclasts [TRAP$^+$ MNCs (multinucleated cells) with $\geqslant 3$ nuclei] growing on a 24-well plate reached at least 3.8 in a random view in each group with no significant difference among the groups of Mock, Lenti-LacZ, Lenti-c1s3 and Lenti-a3 (Figure 3C). The percentage of TRAP$^+$ MNCs ($\geqslant 3$ nuclei) in all TRAP$^+$ cells was also not significantly different among these groups (Figure 3D). These observations indicate that normal differentiation and maturation is sustained in osteoclasts lacking C1 by *C1* knockdown. Taken together, the TRAP staining analysis suggests that knockdown of *C1* does not impair differentiation and maturation of osteoclasts.

Depletion of *Atp6v1c1* blocks osteoclast acidification activity and decreases bone resorption of osteoclasts

We have detected C1, but not C2a or C2b, expressed in osteoclasts. Furthermore, C1 expression was highly induced by RANKL and M-CSF during osteoclast differentiation (Figures 1C–1F), so we postulated that C1 may play a role as an essential component of the

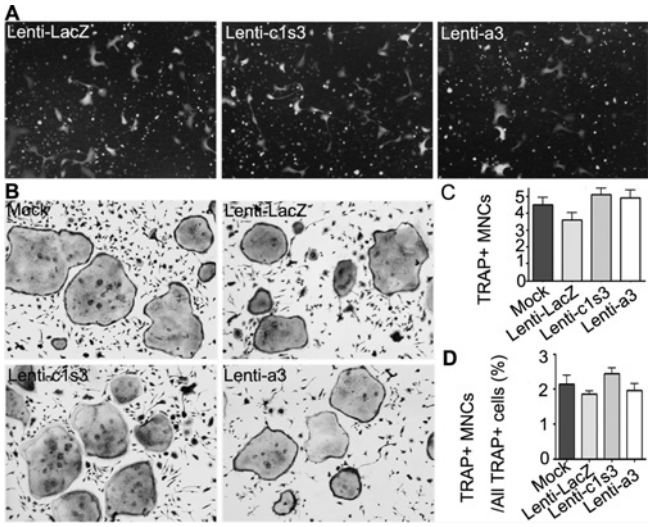

Figure 3 Normal differentiation and maturation of osteoclasts depleted of *Atp6v1c1*

(**A**) All cells expressed GFP, showing that cells were infected by lentivirus and also expressed siRNA. (**B**) TRAP staining of osteoclasts. (**C**) Quantification of TRAP$^+$ OCLs ($\geqslant 3$ nuclei) per random view. (**D**) The percentage of TRAP$^+$ OCLs ($\geqslant 3$ nuclei) in all TRAP$^+$ cells per random view. All data are expressed as means $\pm$ S.D. ($n = 10$).

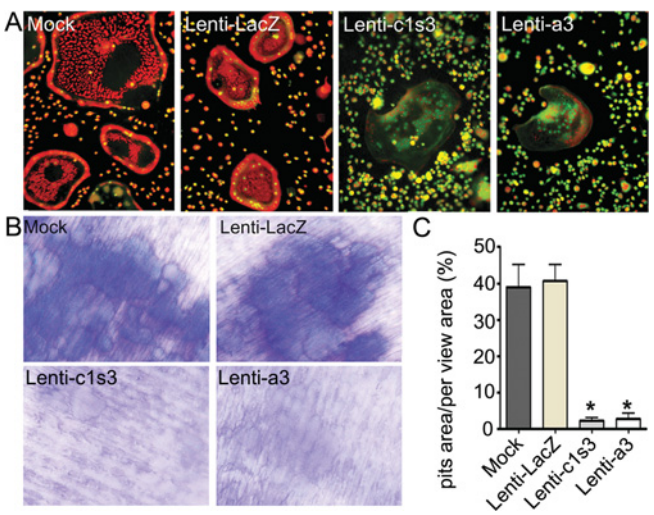

Figure 4 Depletion of *Atp6v1c1* blocked the acidification activity of osteoclasts and decreased bone resorption of osteoclasts

(**A**) Acridine Orange staining of osteoclasts including cells without fusion (<3 nuclei). (**B**) Patterns of resorption pits on dentin slices. (**C**) Quantification of resorption area per view area. Results are mean $\pm$ S.E.M. ($n = 3$). $^*P < 0.05$ compared with that of Lenti-LacZ-treated cells.

osteoclast ruffled border V-ATPase. Therefore we further tested the effect of depletion of C1 on osteoclast acidification activity and bone resorption ability using lentiviral constructs encoding siRNA targeting *Atp6v1c1* and *Atp6v0a3* (as a knockdown control) to infect osteoclasts in primary culture. After infection, we measured the acidification activity by vital staining of osteoclasts with Acridine Orange [32]. In the mock and Lenti-LacZ control osteoclasts, a strong orange/red fluorescence indicated active production of H$^+$ and extracellular acidification (Figure 4A). In comparison, the Lenti-c1s3- and Lenti-a3-treated osteoclasts both displayed little orange/red staining. This result indicates a

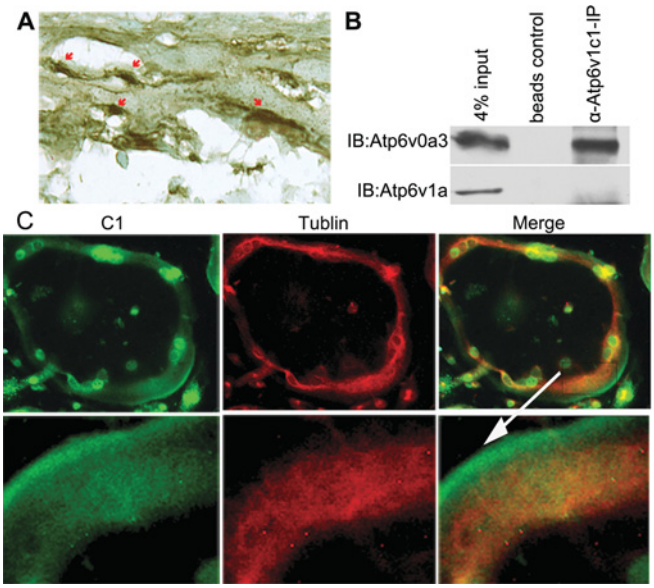

Figure 5 Atp6v1c1 interacted with a3 in osteoclasts and localized towards the bone surface *in vivo* in activated osteoclasts

(**A**) Anti-Atp6v1c1 immunostaining of 10-day-old mouse tibiae. Atp6v1c1 was much more highly expressed in multinucleated osteoclasts and the main staining is at the ruffled border (red arrow). (**B**) Co-IP of Atp6v1c1 with a3 or Atp6v1a. An interaction was observed between C1 and a3 subunits, but no interaction was observed between C1 and A subunits. IB, immunoblot; IP, immunoprecipitation. (**C**) Atp6v1c1 co-localized with microtubules and polarized to the plasma membrane and its vicinity in mature osteoclasts and C1 staining formed a belt at the cell periphery. The cells shown are representative of three experiments.

block of acidification activity owing to the knockdown of *C1* and also *a3*, similar to previous results [13]. Furthermore, we reasoned that C1 may play a role like a3 in osteoclast bone resorption, the major function of osteoclasts. To examine potential functions of C1 in bone resorption, we then assessed resorption pit formation by C1-knockdown osteoclasts on dentin slices. As shown in Figure 4(B), we found reduced pit formation of osteoclasts depleted of *Atp6v1c1* on dentin slices, which is similar to reduced pit formation of osteoclasts depleted of *a3* on dentin slices. Furthermore, pit depth of C1-depleted osteoclasts and a3-depleted osteoclasts are both much shallower than that of normal osteoclasts. We then assessed the percentage of pit area in a view area and found that the percentages in two control groups (mock and Lenti-LacZ) were both approx. 40 %. In contrast, siRNA-treated osteoclasts formed pit areas accounting for only 0.2–0.3 % of a view area (Figure 4C). Taken together, these results strongly suggest that C1, like a3, is an essential component of the ruffled border V-ATPase for the function of osteoclasts.

Atp6v1c1 localizes *in vivo* in activated osteoclasts, it co-localizes with microtubules only in the cytoplasm *in vitro* in mature osteoclasts, and it interacts with a3 in osteoclasts

We found that C1 depletion severely impaired osteoclast acidification and bone resorption (Figures 4A and 4B). So, we further defined whether C1 is a component of the osteoclast ruffled border proton pump. To address this question, we tested C1 localization *in vivo* in activated osteoclasts by performing immunostaining analysis and found that C1 expression in osteoclasts was much higher than in the surrounding tissue, and that the main staining was at the ruffled border (Figure 5A). We further performed a co-IP assay and found that C1 interacted with a3, which is another essential subunit of the osteoclast ruffled border V-ATPase, but C1 did not interact with subunit A (Figure 5B). Subunit a3 has been found to co-localize with microtubules in mature osteoclasts but not with F-actin [33], so we tested whether C1 also co-localizes with microtubules. Interestingly, we found that C1 co-localized with microtubules and that the co-localization polarized to the plasma membrane and its vicinity in mature osteoclasts, just as a3 had previously demonstrated. C1 staining, however, was largely in the cell periphery of mature osteoclasts (Figure 5C). Taken together, these results suggest that C1 is a subunit of the osteoclast ruffled border V-ATPase, and that its interaction with the a3 subunit may be involved in linking the V_1 and V_0 domains together.

Depletion of *Atp6v1c1* blocks osteoclast F-actin ring formation

In bone, the osteoclast cytoskeleton is reorganized during the transition from a motile to a resorbing cell to form an F-actin ring that contains a tight sealing zone [34]. Atp6v0d2 has been reported to be involved in the formation of F-actin rings [20]. Some researchers have reported that Atp6v0a3 is also involved in F-actin ring formation [22], whereas others have reported that a3-deficient osteoclasts have normal F-actin rings [21]. *In vitro* subunit C can cross-link actin filaments to bundles of varying thickness [23]. In the present study, we found that bone resorption was severely impaired in C1-depleted osteoclasts (Figure 4B). Interestingly, C1 largely localized in the cell periphery as a belt in mature osteoclasts (Figure 5C). Therefore we speculated that the reduced acidification activity of *C1*-depleted osteoclasts and their probable inability to form normal F-actin sealing rings would contribute to their reduced bone resorption (Figure 4A). To study the effect of *C1* knockdown on osteoclast actin sealing ring formation, we performed phalloidin staining for F-actin rings. As shown in Figure 6, stained organized F-actin belts at the cell periphery were seen in osteoclasts of control groups (mock, lenti-LacZ, Lenti-a3 and $a3^{-/-}$ osteoclasts), but disorganized F-actin-containing patches were commonly found in *C1*-knockdown osteoclasts (indicated by white arrows). In each cell with an F-actin ring, there were at least three nuclei stained by DAPI. Our results indicated that C1 deficiency severely impaired F-actin ring formation and a3 deficiency did not affect F-actin ring formation.

Atp6v1c1 co-localizes with F-actin in osteoclasts

According to our interesting finding that C1-depleted osteoclasts showed defective F-actin rings (Figure 6) and C1 staining was largely in the cell periphery as a belt (Figure 5C), we further wondered whether C1 and F-actin co-localize in osteoclasts. To address this question, we performed immuofluorescence as shown in Figures 7(A)–7(L). Besides their co-localization in the cytoplasm (Figures 7D, 7G and 7H; single grey arrow), C1 localization moved to the cell periphery along with the F-actin ring (double grey arrow) in mature activated multinuclear osteoclasts. In contrast, C1 and F-actin only co-localized in the cytoplasm in $TRAP^+$ mononuclear cells (Figures 7I–7L). Therefore the destroyed F-actin rings in C1-depleted osteoclasts and the C1 co-localization with F-actin rings, suggest that subunit C1 may be involved in actin sealing ring formation in activated osteoclasts.

DISCUSSION

In the present study we demonstrate that Atp6v1c1 expression is induced by RANKL and M-CSF during osteoclast differentiation, that *Atp6v1c1* silencing can impair osteoclast acidification activity and bone resorption function, that C1 localizes on the ruffled border *in vivo* in activated osteoclasts, that C1 co-localizes with

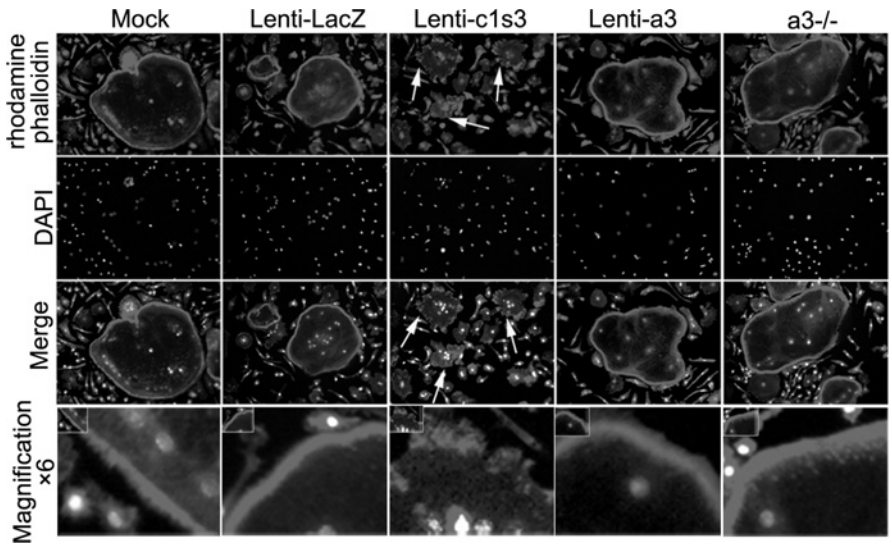

Figure 6 Depletion of Atp6v1c1 blocked F-actin ring formation

Lentivirus-treated cells and a3$^{-/-}$ osteoclasts were stained with rhodamine phalloidin for F-actin rings. Nuclei were visualized with DAPI. F-actin-containing patches are commonly found in C1-knockdown osteoclasts (white arrows), which unlike mock, Lenti-a3- or Lenti-LacZ-infected osteoclasts, or a3$^{-/-}$ osteoclasts, fail to develop an organized actin belt at the cell periphery. The cells shown are representative of four experiments.

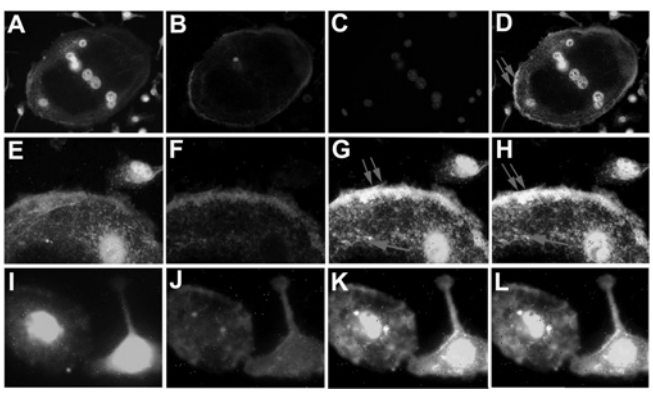

Figure 7 Atp6v1c1 co-localization with F-actin in osteoclasts

(**A**, **E** and **I**) Staining with anti-Atp6v1c1. (**A**) Mature osteoclast. (**E**) Higher magnification of (**A**). (**I**) Mononuclear TRAP^{+} cells. (**B**, **F** and **J**) F-actin rhodamine phalloidin staining. (**B**) Mature osteoclast. (**F**) Higher magnification of (**B**). (**J**) Mononuclear TRAP^{+} cells. (**C**) Nuclei were visualized with DAPI. (**D**) The merge of (**A**), (**B**) and (**C**). (**G**) The merge of (**E**) and (**F**). (**H**) The merge of (**G**) and nuclei. (**K**) The merge of (**I**) and (**J**). (**L**) The merge of (**K**) and nuclei. Besides the co-localization in the cytoplasm (single grey arrow; **D**, **G** and **H**), Atp6v1c1 localization moved to the cell periphery along with the F-actin ring (double grey arrows) in mature multinucleated osteoclasts. In TRAP^{+} mononuclear cells, C1 and F-actin co-localized in the cytoplasm evenly (**K** and **L**). The cells shown are representative of three experiments.

microtubules in mature osteoclasts and strongly interacts with a3, that organized F-actin ring formation is defective in C1-depleted osteoclasts, and that C1 co-localizes with the F-actin ring in osteoclasts. Although the subunit C1 expression pattern in mouse tissues [10] and the subunit C bundles of F-actin of varying thickness *in vitro* [23,24] have been reported, this is the first report to demonstrate that Atp6v1c1 is an essential C subunit of the activated osteoclast ruffled border V-ATPase and that it may regulate F-actin sealing ring formation during osteoclast activation.

Our microarray data showed that, although Atp6v1c2 was weakly detected, Atp6v1c1 was much more highly expressed (approx. 139-fold) than Atp6v1c2 in osteoclasts (Figure 1A), and that Atp6v1c1 expression was 42-fold higher in osteoclasts than in stromal cells (Figure 1B). Sun-Wada et al. [10,16] reported that the subunit Atp6v1c1 was ubiquitously expressed in various tissues in mice, but that the other two C subunit isoforms, C2-a and C2-b, were expressed specifically in the lung and kidney respectively. Therefore we further performed semi-quantitative RT–PCR assays in mouse tissues and cell lines, and verified the higher expression of Atp6v1c1 in osteoclasts. Although we have detected Atp6v1c1 expression in brain, kidney and testis, expression of Atp6v1c1 was much higher in OCLs and osteoclasts than in MOCP-5 and BMMs respectively. In addition, only Atp6v1c1 (not C2-a or C2-b) was detected in osteoclasts, although Atp6v1c2 was detected in the brain, lung, kidney and ES cells (Figures 1C and 1D).

Semi-quantitative assays showed that Atp6v1c1 expression can be significantly induced by RANKL and M-CSF (Figure 1D). Furthermore, our Western blot analysis results also showed that in the osteoclast primary culture, C1 protein continued to increase through day 4 and stayed at high levels until 7 days after BMMs were treated with RANKL and M-CSF (Figures 1E and 1F). In the present study, we report for the first time that C1 (but not C2) is highly expressed in osteoclasts, and that C1 expression can be significantly induced by RANKL and M-CSF.

The high, inducible expression of Atp6v1c1 in osteoclasts provides evidence that C1 may play a role during osteoclast differentiation, maturation and activation. To address this question, we knocked down the expression of Atp6v1c1 using a lentivirus-mediated siRNA expression system [27,28,35], and using both a3-siRNA and LacZ-siRNA as controls. The results showed that C1-knockdown osteoclasts have normal differentiation and maturation, but impaired acidification activity and bone resorption function (Figures 3A–3D and 4A–4C). This was similar to a3-depleted osteoclasts and is also co-incident with the previous report that a3-knockout mice show normal osteoclast maturation, but decreased extracellular acidification and bone resorption [13]. Our results strongly suggest that Atp6v1c1 may play a role as an essential component of the osteoclast ruffled border V-ATPase holoenzyme.

During osteoclast activation, V-ATPases polarize to the ruffled border [1], so we performed immunohistochemistry to verify whether C1 also localized *in vivo* in activated osteoclasts ruffled border. Here, we found that the C1 subunit is much more highly expressed in multinucleated osteoclasts than in surrounding cells and that the main staining was at the ruffled border in activated osteoclasts *in vivo* (Figure 5A, red arrow). As we know, V-ATPase consists of the V_1 and V_0 domains. The V_1 and V_0 domains are connected by a central stalk (composed of subunits D and F of V_1 and subunit d of V_0) and by multiple peripheral stalks (composed of subunits C, E, G and H and the N-terminal domain of subunit a) [2]. Furthermore, the V-ATPase is a tightly coupled enzyme that only exhibits activity when the enzyme is fully assembled with all subunits at the membrane. In yeast, as well as in the tobacco hornworm, subunit C is lost from both sectors during V-ATPase disassociation, suggesting that subunit C may play a crucial role in the regulation of V-ATPases [36–38]. It has been reported that subunit C interacted with subunit a in yeast [39]. Here, we also found that in osteoclasts, subunit C1 strongly interacted with a3 by immunoprecipitation (Figure 5B) and that C1, similar to a3 and Atp6v1a, co-localized with microtubules in osteoclasts and their co-localization polarized to the plasma membrane and its vicinity (Figure 5C) [15,40]. C1 has also been shown to interact with subunit B2 (not B1) in mice [16]. These findings provided further evidence that C1 is an essential component of the osteoclast ruffled border V-ATPase and that its interaction with B2 and a3 may be significant in the connection between V_1 and V_0 domains.

Osteoclastic bone resorption includes two stages: (i) V-ATPases present in the ruffled border secrete H^+ into the compartment surrounded by the sealing zone, thus they provide the acidic microenvironment that leads to bone demineralization; this is followed by (ii) subsequent degradation of the bone matrix by cathepsin K and matrix metalloproteinases that are secreted into the sealing zone [41]. The sealing zone is associated with a ring of actin filaments [18,42]. Tehrani et al. [35] also reported that cortactin-based actin assembly is necessary for the sealing ring to function because cortactin-depleted osteoclasts fail to form actin-based sealing rings and fail to resorb bone. Taken together, F-actin assembly to form organized rings is necessary for the osteoclast bone resorption function. In addition, Vitavska et al. [24] previously reported that in the tobacco hornworm, upon V-ATPase dissociation, V_1 complexes not only detach from the membrane, but also from actin filaments due to the loss of subunit C. Subunit C can bind separately to F-actin, stabilize F-actin, increase the initial rate of actin polymerization in a concentration-dependent manner, and cross-link actin filaments to bundles of varying thickness [23,24]. Their results promote speculation that, in addition to the function of Atp6v1c1 as an essential subunit of the ruffled border V-ATPase, it may be involved in F-actin assembly to form sealing rings in osteoclasts. To test our hypothesis, we depleted *Atp6v1c1* from osteoclasts using RNAi delivered with lentivirus. It is interesting that Atp6v1c1-depleted osteoclasts did not form organized actin rings and that F-actin-containing patches were commonly found in these osteoclasts. In contrast, organized F-actin rings were formed in multinuclear osteoclasts of control groups including Mock, Lenti-LacZ- and Lenti-a3-treated cells, and $a3^{-/-}$ osteoclasts (Figure 6). Our finding that a3-deleted osteoclasts formed normal F-actin rings is co-incident with that in $a3^{-/-}$ osteoclasts; it also supports the previous report that Atp6v0a3-deficient osteoclasts form normal F-actin rings [22]. Therefore it is true that a3 is not involved in F-actin ring formation, which is also consistent with the report that a3 did not co-localize with F-actin rings [15].

Atp6v1c1 deficiency severely impaired F-actin ring formation, so we speculated that C1 co-localizes with F-actin. We performed immunofluorescence to detect C1 and F-actin localization. Besides their co-localization in the cytoplasm (Figures 7A–7L), we found that C1 and F-actin ring localization significantly polarized to the cell periphery in mature multinuclear osteoclasts. In contrast, C1 and F-actin co-localized evenly in the cytoplasm (Figures 7I–7L) in $TRAP^+$ mononuclear cells. The co-localization of C1 and F-actin in osteoclasts suggested that besides being an essential subunit of the V-ATPase, C1 may function as a regulator in normal F-actin ring formation of activated osteoclasts.

The results of the present study show, for the first time, that Atp6v1c1 plays a role in osteoclast bone resorption as an essential C subunit and may also function as a regulator of F-actin sealing ring formation during osteoclast activation. Furthermore, its expression can be induced by RANKL and M-CSF during osteoclast differentiation, so further studies will be required to identify other molecules that might be involved in the signal pathway by which RANKL and M-CSF activate osteoclasts to form the F-actin sealing ring through C1. Our results showed a high level of C1 expression induced by RANKL (Figure 1E) and an undetectable level of C1 expression in other cells in bone marrow (Figures 1B, 1C, 1E and 5A). So, we suggest that Atp6v1c1 would be a useful target for diseases of bone and cartilage if it is possible to knockdown C1 expression specifically in bone marrow cells by an approach such as C1 shRNA lentivirus infection of bone marrow *in vivo* (as we did *in vitro*; Figure 3).

We thank Christie Taylor and Carrie Soltanoff for their assistance with the manuscript before submission. This work was supported by the fund provided by Zhejiang Cell Biomedical Research College, CSC (China Scholarship Council) and NIH (National Institutes of Health) Grant AR-44741 (to Y.-P. L.).

REFERENCES

1 Xu, J., Cheng, T., Feng, H. T., Pavlos, N. J. and Zheng, M. H. (2007) Structure and function of V-ATPases in osteoclasts: potential therapeutic targets for the treatment of osteolysis. Histol. Histopathol. **22**, 443–454
2 Forgac, M. (2007) Vacuolar ATPases: rotary proton pumps in physiology and pathophysiology. Nat. Rev. Mol. Cell Biol. **8**, 917–929
3 Forgac, M. (1999) Structure and properties of the vacuolar H^+-ATPases. J. Biol. Chem. **274**, 12951–12954
4 Xu, T., Vasilyeva, E. and Forgac, M. (1999) Subunit interactions in the clathrin-coated vesicle vacuolar H^+-ATPase complex. J. Biol. Chem. **274**, 28909–28915
5 Stevens, T. H. and Forgac, M. (1997) Structure, function and regulation of the vacuolar H^+-ATPase. Annu. Rev. Cell Dev. Biol. **13**, 779–808
6 Nishi, T., Kawasaki-Nishi, S. and Forgac, M. (2003) Expression and function of the mouse V-ATPase d subunit isoforms. J. Biol. Chem. **278**, 46396–46402
7 Paunescu, T. G., Da, S. N., Marshansky, V., McKee, M., Breton, S. and Brown, D. (2004) Expression of the 56-kDa B2 subunit isoform of the vacuolar H^+-ATPase in proton-secreting cells of the kidney and epididymis. Am. J. Physiol. Cell Physiol. **287**, C149–C162
8 Pietrement, C., Sun-Wada, G. H., Silva, N. D., McKee, M., Marshansky, V., Brown, D., Futai, M. and Breton, S. (2006) Distinct expression patterns of different subunit isoforms of the V-ATPase in the rat epididymis. Biol. Reprod. **74**, 185–194
9 Smith, A. N., Borthwick, K. J. and Karet, F. E. (2002) Molecular cloning and characterization of novel tissue-specific isoforms of the human vacuolar H^+-ATPase C, G and d subunits, and their evaluation in autosomal recessive distal renal tubular acidosis. Gene **297**, 169–177
10 Sun-Wada, G. H., Yoshimizu, T., Imai-Senga, Y., Wada, Y. and Futai, M. (2003) Diversity of mouse proton-translocating ATPase: presence of multiple isoforms of the C, d and G subunits. Gene **302**, 147–153
11 Murata, Y., Sun-Wada, G. H., Yoshimizu, T., Yamamoto, A., Wada, Y. and Futai, M. (2002) Differential localization of the vacuolar H^+ pump with G subunit isoforms (G1 and G2) in mouse neurons. J. Biol. Chem. **277**, 36296–36303
12 Lee, B. S., Holliday, L. S., Ojikutu, B., Krits, I. and Gluck, S. L. (1996) Osteoclasts express the B2 isoform of vacuolar H^+-ATPase intracellularly and on their plasma membranes. Am. J. Physiol. **270**, C382–C388

13 Li, Y. P., Chen, W., Liang, Y., Li, E. and Stashenko, P. (1999) Atp6i-deficient mice exhibit severe osteopetrosis due to loss of osteoclast-mediated extracellular acidification. Nat. Genet. **23**, 447–451

14 Kornak, U., Kasper, D., Bosl, M. R., Kaiser, E., Schweizer, M., Schulz, A., Friedrich, W., Delling, G. and Jentsch, T. J. (2001) Loss of the CLC-7 chloride channel leads to osteopetrosis in mice and man. Cell **104**, 205–215

15 Toyomura, T., Murata, Y., Yamamoto, A., Oka, T., Sun-Wada, G. H., Wada, Y. and Futai, M. (2003) From lysosomes to the plasma membrane: localization of vacuolar-type H^+-ATPase with the a3 isoform during osteoclast differentiation. J. Biol. Chem. **278**, 22023–22030

16 Sun-Wada, G. H., Murata, Y., Namba, M., Yamamoto, A., Wada, Y. and Futai, M. (2003) Mouse proton pump ATPase C subunit isoforms (C2-a and C2-b) specifically expressed in kidney and lung. J. Biol. Chem. **278**, 44843–44851

17 Faccio, R., Grano, M., Colucci, S., Villa, A., Giannelli, G., Quaranta, V. and Zallone, A. (2002) Localization and possible role of two different $\alpha V\beta 3$ integrin conformations in resting and resorbing osteoclasts. J. Cell Sci. **115**, 2919–2929

18 Saltel, F., Destaing, O., Bard, F., Eichert, D. and Jurdic, P. (2004) Apatite-mediated actin dynamics in resorbing osteoclasts. Mol. Biol. Cell **15**, 5231–5241

19 Pfaff, M. and Jurdic, P. (2001) Podosomes in osteoclast-like cells: structural analysis and cooperative roles of paxillin, proline-rich tyrosine kinase 2 (Pyk2) and integrin $\alpha V\beta 3$. J. Cell Sci. **114**, 2775–2786

20 Lee, S. H., Rho, J., Jeong, D., Sul, J. Y., Kim, T., Kim, N., Kang, J. S., Miyamoto, T., Suda, T., Lee, S. K. et al. (2006) v-ATPase V0 subunit d2-deficient mice exhibit impaired osteoclast fusion and increased bone formation. Nat. Med. **12**, 1403–1409

21 Hu, Y., Nyman, J., Muhonen, P., Vaananen, H. K. and Laitala-Leinonen, T. (2005) Inhibition of the osteoclast V-ATPase by small interfering RNAs. FEBS Lett. **579**, 4937–4942

22 Taranta, A., Migliaccio, S., Recchia, I., Caniglia, M., Luciani, M., De Rossi, G., Dionisi-Vici, C., Pinto, R. M., Francalanci, P., Boldrini, R. et al. (2003) Genotype–phenotype relationship in human ATP6i-dependent autosomal recessive osteopetrosis. Am. J. Pathol. **162**, 57–68

23 Vitavska, O., Merzendorfer, H. and Wieczorek, H. (2005) The V-ATPase subunit C binds to polymeric F-actin as well as to monomeric G-actin and induces cross-linking of actin filaments. J. Biol. Chem. **280**, 1070–1076

24 Vitavska, O., Wieczorek, H. and Merzendorfer, H. (2003) A novel role for subunit C in mediating binding of the H^+-V-ATPase to the actin cytoskeleton. J. Biol. Chem. **278**, 18499–18505

25 Yang, S. and Li, Y. P. (2007) RGS12 is essential for RANKL-evoked signaling for terminal differentiation of osteoclasts *in vitro*. J. Bone Miner. Res. **22**, 45–54

26 Chen, W. and Li, Y. P. (1998) Generation of mouse osteoclastogenic cell lines immortalized with SV40 large T antigen. J. Bone Miner. Res. **13**, 1112–1123

27 Kissler, S., Stern, P., Takahashi, K., Hunter, K., Peterson, L. B. and Wicker, L. S. (2006) *In vivo* RNA interference demonstrates a role for Nramp1 in modifying susceptibility to type 1 diabetes. Nat. Genet. **38**, 479–483

28 Stewart, S. A., Dykxhoorn, D. M., Palliser, D., Mizuno, H., Yu, E. Y., An, D. S., Sabatini, D. M., Chen, I. S., Hahn, W. C., Sharp, P. A. et al. (2003) Lentivirus-delivered stable gene silencing by RNAi in primary cells. RNA **9**, 493–501

29 Murrills, R. J. and Dempster, D. W. (1990) The effects of stimulators of intracellular cyclic AMP on rat and chick osteoclasts *in vitro*: validation of a simplified light microscope assay of bone resorption. Bone **11**, 333–344

30 Yang, S., Chen, W., Stashenko, P. and Li, Y. P. (2007) Specificity of RGS10A as a key component in the RANKL signaling mechanism for osteoclast differentiation. J. Cell Sci. **120**, 3362–3371

31 Yang, S. and Li, Y. P. (2007) RGS10-null mutation impairs osteoclast differentiation resulting from the loss of $[Ca^{2+}]i$ oscillation regulation. Genes Dev. **21**, 1803–1816

32 Baron, R., Neff, L., Louvard, D. and Courtoy, P. J. (1985) Cell-mediated extracellular acidification and bone resorption: evidence for a low pH in resorbing lacunae and localization of a 100-kD lysosomal membrane protein at the osteoclast ruffled border. J. Cell Biol. **101**, 2210–2222

33 Toyomura, T., Oka, T., Yamaguchi, C., Wada, Y. and Futai, M. (2000) Three subunit a isoforms of mouse vacuolar H^+-ATPase. Preferential expression of the a3 isoform during osteoclast differentiation. J. Biol. Chem. **275**, 8760–8765

34 Blair, H. C., Teitelbaum, S. L., Ghiselli, R. and Gluck, S. (1989) Osteoclastic bone resorption by a polarized vacuolar proton pump. Science **245**, 855–857

35 Tehrani, S., Faccio, R., Chandrasekar, I., Ross, F. P. and Cooper, J. A. (2006) Cortactin has an essential and specific role in osteoclast actin assembly. Mol. Biol. Cell **17**, 2882–2895

36 Parra, K. J., Keenan, K. L. and Kane, P. M. (2000) The H subunit (Vma13p) of the yeast V-ATPase inhibits the ATPase activity of cytosolic V1 complexes. J. Biol. Chem. **275**, 21761–21767

37 Kane, P. M. (1995) Disassembly and reassembly of the yeast vacuolar H^+-ATPase *in vivo*. J. Biol. Chem. **270**, 17025–17032

38 Sumner, J. P., Dow, J. A., Earley, F. G., Klein, U., Jager, D. and Wieczorek, H. (1995) Regulation of plasma membrane V-ATPase activity by dissociation of peripheral subunits. J. Biol. Chem. **270**, 5649–5653

39 Inoue, T. and Forgac, M. (2005) Cysteine-mediated cross-linking indicates that subunit C of the V-ATPase is in close proximity to subunits E and G of the V1 domain and subunit a of the V0 domain. J. Biol. Chem. **280**, 27896–27903

40 Abu-Amer, Y., Ross, F. P., Schlesinger, P., Tondravi, M. M. and Teitelbaum, S. L. (1997) Substrate recognition by osteoclast precursors induces C-src/microtubule association. J. Cell Biol. **137**, 247–258

41 Henriksen, K., Sorensen, M. G., Nielsen, R. H., Gram, J., Schaller, S., Dziegiel, M. H., Everts, V., Bollerslev, J. and Karsdal, M. A. (2006) Degradation of the organic phase of bone by osteoclasts: a secondary role for lysosomal acidification. J. Bone Miner. Res. **21**, 58–66

42 Kanehisa, J., Yamanaka, T., Doi, S., Turksen, K., Heersche, J. N., Aubin, J. E. and Takeuchi, H. (1990) A band of F-actin containing podosomes is involved in bone resorption by osteoclasts. Bone **11**, 287–293

Received 28 May 2008/23 July 2008; accepted 25 July 2008
Published on the Internet 12 December 2008, doi:10.1042/BJ20081073